

# Design and Prototyping of a Bio-Inspired Kinematic Sensing Suit for the Shoulder Joint: Precursor to a Multi-DoF Shoulder Exosuit

Rejin John Varghese<sup>✉</sup>, Benny Ping Lai Lo<sup>✉</sup>, and Guang-Zhong Yang, *Fellow, IEEE*

**Abstract**—Soft wearable robots represent a promising new design paradigm for rehabilitation and active assistance applications. Their compliant nature makes them ideal for complex joints, but intuitive control of these robots require robust and compliant sensing mechanisms. In this work, we introduce the sensing framework for a multiple degrees-of-freedom shoulder exosuit capable of sensing the kinematics of the joint. The proposed sensing system is inspired by the body’s embodied kinematic sensing, and the organisation of muscles and muscle synergies responsible for shoulder movements. A motion-capture-based evaluation study of the developed framework confirmed conformance with the behaviour of the muscles that inspired its routing. This validation of the tendon-routing hypothesis allows for it to be extended to the actuation framework of the exosuit in the future. The sensor-to-joint-space mapping is based on multivariate multiple regression and derived using an Artificial Neural Network. Evaluation of the derived mapping achieved root mean square error of  $\approx 5.43^\circ$  and  $\approx 3.65^\circ$  for the azimuth and elevation joint angles measured over 29,500 frames (4+ minutes) of motion-capture data.

**Index Terms**—Medical robots and systems, prosthetics and exoskeletons, biomimetics, wearable robots, soft robot materials and design.

## I. INTRODUCTION

A SIGNIFICANT fraction of the world population suffers from conditions affecting motor function. Additionally, longevity will lead to increasing ageing-related debilitating muscular manifestations [1]. The rising demand for time-consuming, expensive and repetitive rehabilitation therapy and assistance traditionally provided by therapists and care workers is now making way for robot-based therapy and exoskeletons [2]–[4]. Rigid-bodied exoskeleton designs inherently have limitations that include increased size/weight, lack of compliance,

Manuscript received September 10, 2019; accepted December 12, 2019. Date of publication January 3, 2020; date of current version January 14, 2020. This letter was recommended for publication by Associate Editor Lorenzo De Micheli and Editor Pietro Valdastri upon evaluation of the reviewers’ comments. This research is supported by Future AI and Robotics for Space (FAIR-SPACE) under Grant EP/R026092/1 awarded by EPSRC, U.K. (*Corresponding author: Rejin John Varghese*.)

R. J. Varghese is with the Hamlyn Centre, Imperial College London, U.K. and also with the Department of Computing, Imperial College London, U.K. (e-mail: r.varghese15@imperial.ac.uk).

B. P. L. Lo is with the Hamlyn Centre, Imperial College London, U.K. (e-mail: benny.lo@imperial.ac.uk).

G.-Z. Yang is with the Institute of Medical Robotics, Shanghai Jiao Tong University, China (e-mail: gzyang@sjtu.edu.cn).

This letter has supplementary downloadable material available at <http://ieeexplore.ieee.org>, provided by the authors.

Digital Object Identifier 10.1109/LRA.2019.2963636

restrictive movements, and introducing misalignments [2]–[4]. The challenges faced in laboratory to real-world translation of rigid-bodied exoskeletons and the more universal need for systems that provide partial rather than complete assistance has resulted in a transition towards compliant, portable and wearable systems [2]. A new generation of soft wearable robots leveraging the body’s anatomical structures is making use of unconventional materials and actuation methods for rehabilitation and assistance applications [2], [5]–[8].

The compliant nature of soft exoskeletons (exosuits) makes them ideal for multiple degrees-of-freedom (DoF) joints such as the shoulder that have inherent sources of misalignments. A few soft wearable robotic systems have focussed on 1-DoF (abduction/adduction) assistance for the shoulder [7], [8]. 2-DoF solutions include a semi-rigid continuum robot system [9] and two multi-DoF tendon-driven exosuits [10], [11]. Soft kinematic sensing networks are vital for compensating the compliance and non-linearities inherent in these human-exosuit systems, and needs to work alongside a vision-based system to provide sensory feedback for accomplishing different tasks. This is analogous to the human body where proprioception, sensors in the skin, and vision work together for natural and intuitive upper-limb functionality. Research works have explored different soft kinematics sensing systems including dielectric elastomers [12], micro-fluidics [13], and liquid metal alloys [14], along with traditional sensors such as flex/bend sensors [7] and Inertial Measurement Units (IMUs) [7]. Most of these systems suffer from hysteresis, creep, limited range and other non-linearities. IMUs can achieve high performance, but suffer from drift [7], [15]. IMUs were not considered in this research as our system is also being developed to counteract the muscular atrophy experienced by astronauts during prolonged space travel [16]. IMUs need stable magnetic and gravitational fields to sense joint kinematics reliably.

In this work, we introduce the kinematic sensing framework of our multi-DoF shoulder exosuit which is based on a novel bio-inspired tendon-routing design architecture. The tendon-routing is inspired by the concept of muscle synergies [17], and the sensing modality in the suit tries to replicate the mechanism behind our sense of proprioception [18]. A preliminary simulation-based feasibility study of this framework was presented by the authors in [19]. Tendon-driven systems, analogous to the muscles in our body, can only apply forces while pulling and hence their positioning/routing on the body is crucial. There are

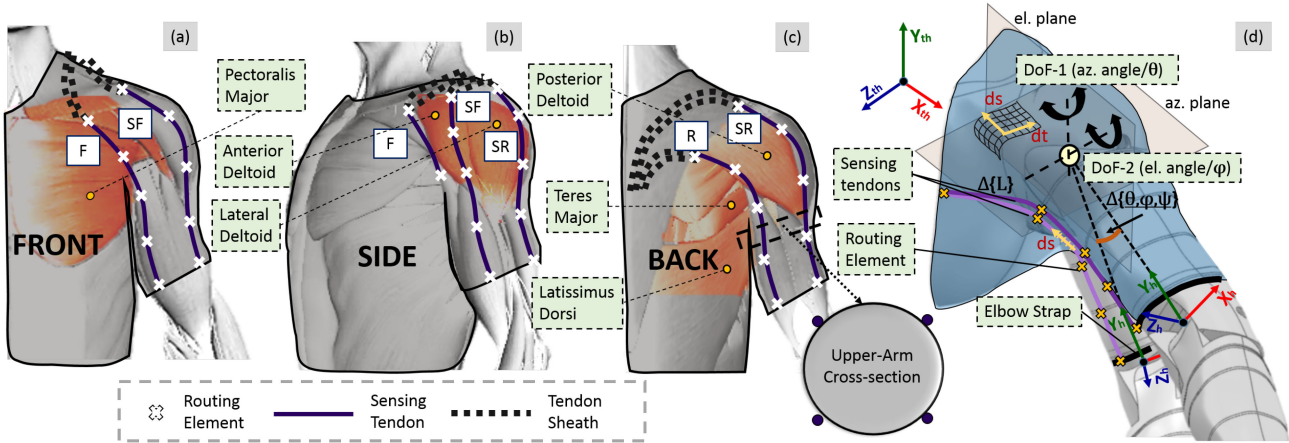


Fig. 1. Sensing framework schematic and principle: a)-c). Layout of the routing of the different tendons ( $F$ ,  $SF$ ,  $SR$ ,  $R$ ) based on the different sets of muscles on the upper-arm. The tendons are routed through 3-D printed elements and tendon-sheaths. A cross-section of the arm with the tendons is also shown. d). Sensing principle: The figure shows the effect of a change in the pose (measured in azimuth and elevation plane) on the change in the lengths of a tendon routed across the shoulder. The blue graphic depicts the shoulder as a 3D surface, and the grid highlights the 2D parametrisation of this 3D surface with parameters  $s$  and  $t$ , and, similarly, the purple tendon on this surface is parametrised as a 1D curve with parameter  $s$ .

many possible combinations of tendon-routing and, this study, therefore, is also a precursory feasibility study for the actuation framework of our exosuit. In the next section, we introduce the bio-inspired tendon routing concept and design of our proposed sensing framework.

## II. SENSING FRAMEWORK DESIGN

### A. The Bio-Inspired Tendon-Routing Architecture

Traditionally, kinematic sensing in a robot is achieved through joint encoders or IMUs, but these solutions cannot be applied to our exosuit. As the suit aims to augment the body, we take inspiration from the kinematic sensing in the body. Proprioception, the “sixth sense,” is the sense of relative position/movement, force/effort, and balance [18]. Muscle spindles in the skeletal muscle act as “stretch receptors” (measuring stretch in the muscles and not joint angles) to get sense of a limb’s position and movement [18], [20].

We hypothesise that a sensing framework based on measuring the stretch/displacement in multiple tendons routed around the shoulder (inspired by the organisation of muscles influencing shoulder movement) could function analogous to the body’s sense of proprioception and provide the exosuit with kinematic sensing capability (Fig. 1).

The glenohumeral (shoulder) joint is a complex joint with 3+ DoFs [21]. In this work, we aim to sense the 2-DoFs (azimuth( $\alpha/\theta$ ) & elevation( $\text{el.}/\phi$ ) angles) that manifest conjointly (Fig. 1(d)). The third DoF (internal/external rotation) manifests at the forearm and can only be measured at the elbow. This choice of shoulder angles is defined by the OpenSim musculoskeletal (MS) model [22] used for inverse kinematics analysis, and is detailed later. Flexion/Extension (F/E), Abduction/Adduction (Ab/Ad) & Horizontal Abduction/Adduction (HAb/HAd) movements are facilitated by 5 sets of muscles (Fig. 1): Chest (Pectoralis major (PM)), Back (Latissimus dorsi (LDo), Teres Major (TM)) and the three deltoid (shoulder heads-Anterior (AD), Lateral (LD) and Posterior (PD)

deltoid [21]. Other muscles such as the biceps, triceps, and brachialis muscles also support shoulder movements [17], [21]. If the tendon routing were to be replicated exactly like the muscles, 5+ tendons would be needed for sensing 2 DoFs making the suit bulky and complex.

To reduce the number of tendons, we take inspiration from the **muscle synergy** concept, proposed by Bernstein [23]. It states that the Central Nervous System simplifies movement control by co-activating a group of muscles responsible for a particular movement as a synergy rather than activating muscles individually. Even though 5+ muscles work together to generate movements in 2-DoFs, 4 muscle synergies can account for these movements [17], [24]. An example of a robotic glove employing a synergy-based design is presented in [5]. We, therefore, attempt a similar dimensionality reduction by routing tendons parallel ( $\parallel$ ) to a set of muscles that work together and propose a tendon-routing architecture made up of 4 tendon-based sensing units-  $F$ ,  $SF$ ,  $SR$ ,  $R$  (Fig. 1):

- Tendon  $F \parallel$  (PM and AD): sensing F/E and HAb/HAd.
- Tendon  $SF \parallel$  (AD and LD): sensing F/E and Ab/Ad.
- Tendon  $SR \parallel$  (LD and PD): sensing F/E and Ab/Ad.
- Tendon  $R \parallel$  (PD, TM and LDo): sensing F/E and HAb/HAd.

The tendons are routed along specific paths on the suit using routing elements (Fig. 1 & 2). When the arm moves, the tendon paths (and associated muscle spindles) shorten/ elongate and is tracked by sensors (Fig. 1(d)). Data from multiple tendons are then fused to derive the joint angles. The sensing framework w.r.t the shoulder’s forward kinematics can be expressed with the following equations. The 3D shoulder surface, a function of  $(\theta, \phi)$ , can be expressed parametrically in 2 independent parameters,  $t$  and  $s$  (Fig. 1(d)):

$$x_{surf} = f_{\theta, \phi}(t, s), y_{surf} = g_{\theta, \phi}(t, s), z_{surf} = h_{\theta, \phi}(t, s) \quad (1)$$

Similarly, the 3D paths of the tendons can be expressed parametrically in 1 independent parameter,  $s$ , as a 1-D curve (cubic

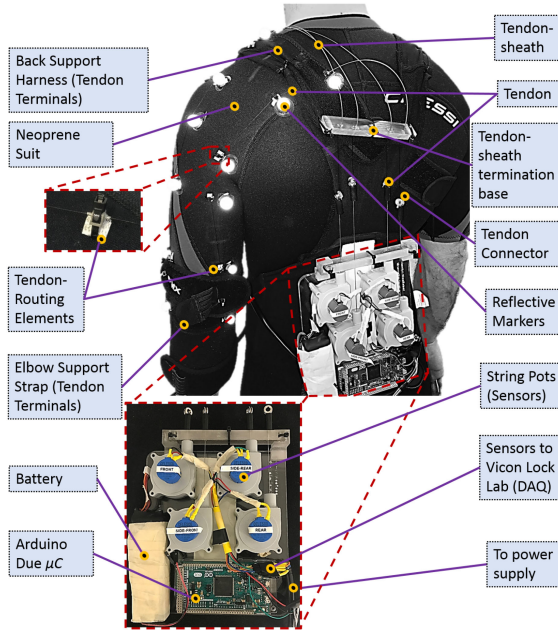


Fig. 2. Overview of the sensing framework prototype for the shoulder exosuit with a description of the electro-mechanical and mechanical elements.

spline) (Fig. 1(d)):

$$x_{tend} = p(s), \quad y_{tend} = q(s), \quad z_{tend} = r(s). \quad (2)$$

Eq.2 will satisfy eq.1 at every point as the tendons and all routing elements lie on the shoulder surface. The path length of the tendons can then be written as:

$$\ell_{tend} = \int d\ell, \text{ where } d\ell = \sqrt{dx_{tend}^2 + dy_{tend}^2 + dz_{tend}^2}. \quad (3)$$

The length of a tendon is a function of  $(\theta, \phi)$  and the sensing framework estimates  $\Delta\ell(\theta, \phi)$

$$\begin{aligned} \ell_{tend} &= L_{tend}(\theta, \phi), \\ \Delta\ell_{tend}(\theta, \phi) &= L_{tend}(\theta, \phi) - L_{tend}(\theta_{init}, \phi_{init}), \end{aligned} \quad (4)$$

where  $(\theta_{init}, \phi_{init})$  are the angles when the arm is in the rest position (neutral) by the side of the body.  $\Delta\ell(\theta, \phi)$  is the metric estimated by each sensor.  $S = \{\Delta\ell_F, \Delta\ell_SF, \Delta\ell_SR, \Delta\ell_R\} \subset \mathbb{R}^4$  represents the sensor space made up of the 4 sensors, and  $q = \{\theta, \phi\} \subset \mathbb{R}^2$  represents the joint-space made up of azimuth and elevation joint angles. In the next section, we discuss the sensor-to-joint-space ( $S \mapsto q$ ) mapping to estimate the two joint angles  $(\theta, \phi)$  from the four sensors.

### B. Sensor-Space to Joint-Space Mapping

To obtain joint angles from real/virtual sensors values, the mapping from sensor-space to joint-space ( $S \mapsto q$ ) needs to be derived. While performing shoulder movement experiments, the joint angles (from motion-capture (MoCap) data) and the corresponding sensor values are recorded and used to derive this mapping. This  $S \mapsto q$  mapping is equivalent to the inverse kinematics solution of the upper-arm in tendon-path space, where the termination point of each tendon can be considered

the tip of the end-effector. This mapping from four sensor to two joint values is a multivariate multiple regression problem and can be solved very effectively by Artificial Neural Networks (ANNs) [19]. The ANN behaves as a sensor fusion mechanism to extract joint kinematics from 4 homologous sensors [19]. A network with 1 hidden layer,  $4 \times 25 \times 2$  neurons, and trained by backpropagation is used. Mathematically, this  $S \mapsto q$  mapping can then be written as:

$$q = A(WS + b), \quad (5)$$

where  $A$  is the activation function,  $W$  the matrix of learned weights, and  $b$  the bias values array.

### C. Hardware Design of the Sensing Suit

To test our hypothesis, a subject-specific suit presented in Fig. 2 was developed. A neoprene compression-fit suit (Cressi, Italy) was chosen as the base layer of the suit as it conforms closely with the skin and can withstand small forces from the tendons. The SUS 304 stainless steel tendons (Asahi Intecc Co. Ltd., Japan) were routed along the lines as discussed previously (Fig. 1). The tendons are routed using 3D-printed routing elements attached to the base layer, and tendon-sheaths (Asahi Intecc Co. Ltd., Japan) in a Bowden-cable arrangement.

The metal routing elements (inset in Fig. 2) were printed using the Mlab Cusing 3D printer (Concept Laser, Germany). These routing elements ensure that the tendons maintain the desired path and adhere closely to the suit, and not follow the shortest line outside the body as seen in [10], [11]. Both tendons (OD  $\phi 0.47$  mm) and the tendon-sheaths (OD  $\phi 1.12$  mm, ID  $\phi 0.55$  mm) were Teflon-coated to reduce friction. Small pieces of tendon-sheaths were also glued to the routing elements to reduce friction and allow smooth transition across the element. Between 4 and 6 elements were used to route each sensing tendon. A wearable back-support and elbow support sleeve (both fastened to the base) were used to support the routing elements that experienced largest forces (tendon termination points and points of exit out of the tendon sheaths). The tendon sheaths were used to route the tendons from the last routing elements to a 3D-printed termination base. This leaves the tendon exposed between the tendon-sheath termination to the origin of the sensor which is a string potentiometer (string-pot) (Fig. 2). The tendons from the string-pots are then connected to the tendons across the shoulder using detachable 3D-printed parts (tendon connectors). This was intentionally done for visual demonstrability of the concept, to act as a mechanical fuse to prevent high forces from being transmitted, and to make the electronics modular and separable.

To measure the displacement of each tendon, its free end is attached to a Celesco SP1-12 string-pot sensor (Intertechnology Inc., Toronto, Canada). The spring in the sensor applies a constant small force ( $\sim 1.9$  N) over a displacement of  $12''$  (30.48 cm). This allows the tendon to be tracked accurately while being small enough to not deform the neoprene and fabric reinforcements excessively or cause the wearer any discomfort. The string-pot uses a potentiometer ( $10\text{ k}\Omega$ ) to measure the displacement through a voltage divider circuit. The analog signals from the four sensors

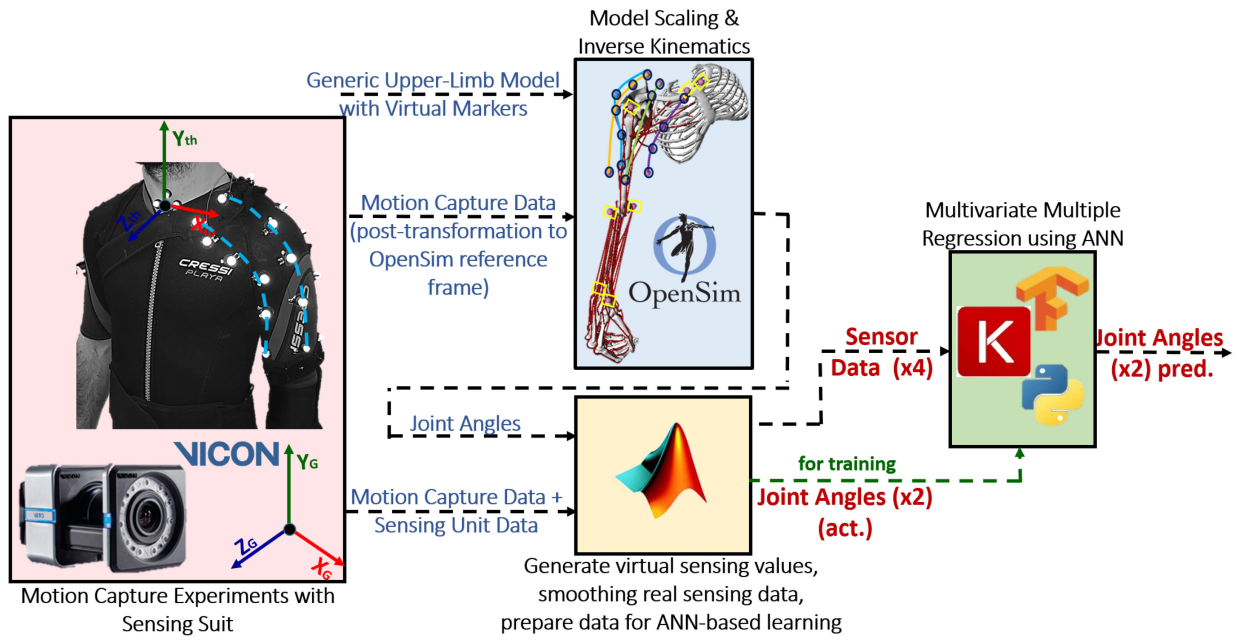


Fig. 3. Overview of the experimental methodology for prototype evaluation: Data from MoCap experiments are processed using both the OpenSim MS modelling software and MATLAB to get joint angle, and real and virtual sensor data. This data is used to train an ANN to predict the joint angles given the 4 sensor values. Virtual sensor lines generated using reflective markers (corresponding to the routing elements) are shown with the cyan-coloured lines.

are read by an Arduino Due (Arduino, Italy) microcontroller ( $\mu$ C) board. The string-pots were powered with 3.3 V, and the ADC on the Arduino  $\mu$ C was set to 12 bits to give the string-pot a theoretical sensor resolution of  $\approx 0.075$  mm. The electronics were mounted on the back support making the entire system portable (Fig. 2). The total weight of the electromechanical components and the base is  $\sim 950$  g, and will be made lighter in future iterations.

### III. CONCEPT EVALUATION EXPERIMENTS

#### A. Experimental Setup

To evaluate our prototype, experiments were performed with MoCap equipment to obtain ground truth data. The experiments were performed under the ethics approval provided by the Imperial College Research Ethics Committee with reference number 18IC4816. We used a lab with 10 Vero 2.2 cameras, a Vue video camera, a Lock Lab and auxiliary equipment from Vicon (Vicon, Oxford, UK) for our experiments. The subject was made to wear the prototype and the reflective markers and electronics were attached. For the MoCap experiments, the sensors were connected directly to the Vicon Lock Lab, a synchronisation device to acquire external analog signal data. The Lock Lab acquired data from the sensors at 1200 Hz and the cameras at 120 Hz. Calibration experiments were performed on the string-pots to estimate displacements from sensor voltages.

#### B. Experimental Methodology

The experiments in this work were performed only on one subject as the tendon-routing architecture was designed specifically based on the physiology and morphology of that subject. To

perform the MoCap experiments, markers were attached adjacent to the 3D-printed routing elements and also on the subject's anatomical features at the clavicle, shoulder and elbow (Fig. 2 & 3). The MoCap data from the anatomical features were used to derive the joint angles of the shoulder. OpenSim, an open-source musculoskeletal (MS) modelling software, was used [25] to derive the same. We used the MoBL-ARMS Dynamic Upper Limb model developed by Saul *et al.* in [22] to solve the inverse kinematics of the shoulder. OpenSim was used to derive joint angles (as opposed to directly using MoCap data) as the shoulder cannot be approximated simply as a ball-and-socket joint [21]. MATLAB (Mathworks, MA, USA) was used to transform the marker data from the Vicon system's reference frame to a local coordinate system on the subject used by OpenSim (Fig. 3). Data from static experiments were used to scale the generic MS model to our subject using OpenSim's Scaling tool. The Inverse Kinematics tool was then applied on data from the dynamic MoCap experiments to derive the two DoFs. The movements performed during MoCap experiments for deriving and validating the  $S \mapsto q$  map is presented in Table I. The table details the movements performed, joint angle ranges/limits during these movements, number of repetitions (reps) performed, and the trial time/frames recorded at 120 Hz. Over 29,500 frames (4+ minutes) of data was obtained. The joint angle convention in this work can be transformed to that of the International Society of Biomechanics with the transformations presented in [26].

The routing elements govern the behaviour of each sensing tendon (see eq. 1–4), and hence were also tracked in the MoCap experiments. Along with real sensor data, virtual sensors were derived using splines defined by joining these markers (dashed cyan lines in Fig. 3). Splines were derived for each sensor for each frame of captured data. The change in length of these

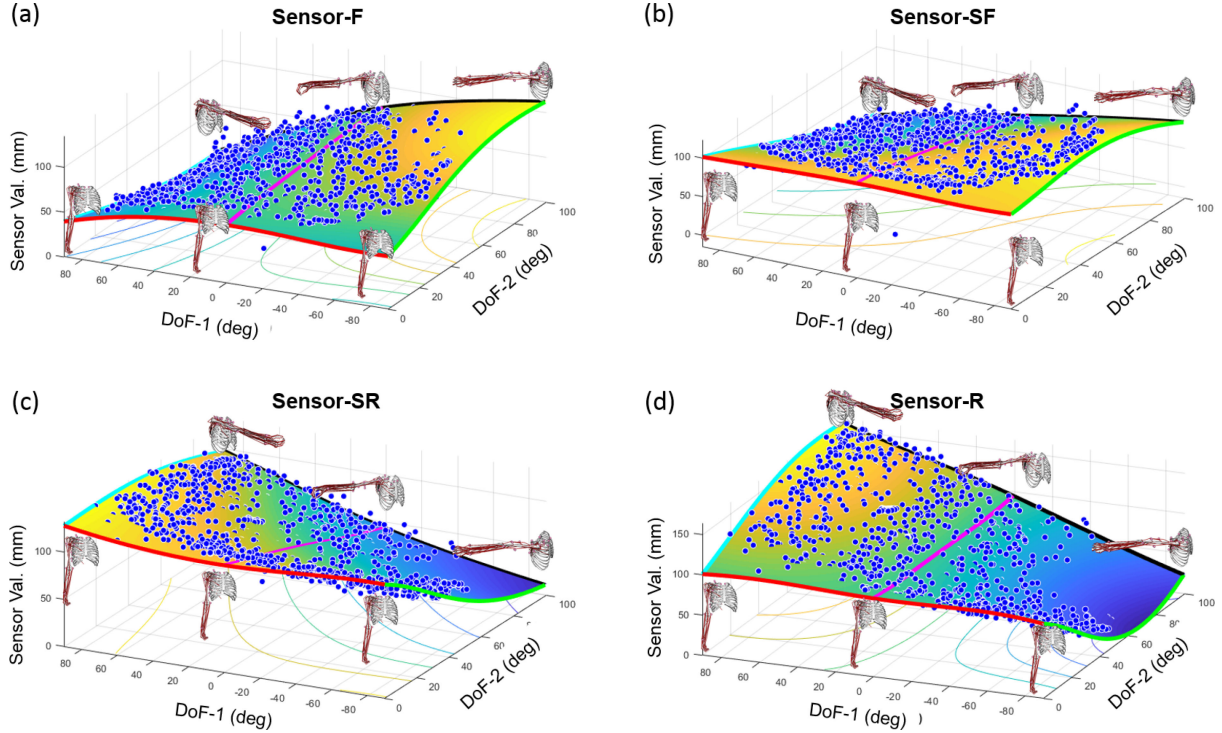


Fig. 4.  $\mathbf{q} \mapsto \mathbf{S}$  Mapping: Change in path lengths measured by the 4 virtual sensors - a).F, b).SF, c).SR and, d).R over entire range of azimuth (DoF-1) and elevation (DoF-2) joint angles. The blue dots are 10% of the sensor values, and the surface plot is the ANN-based  $\mathbf{q} \mapsto \mathbf{S}$  fitting. In the graphs, the cyan and green lines represent F/E movements, the magenta line represents Ab/Ad movements, and the black line represents HAb/HAd movements. The red line represents the neutral position (Gimbal lock in DoF-1). The OpenSim graphics show the upper-limb position at the extremities of each line.

TABLE I  
MOVEMENTS PERFORMED BY SUBJECT DURING MOCAP EXPERIMENTS

Movement	Joint Angles Range/Limits	No. of Reps.	No. of Frames	Trial Time
F/E	$\theta = -90^\circ / 90^\circ$ $0^\circ \leq \phi \leq 90^\circ$	4	3037	25.31s
Ab/Ad	$\theta = 0^\circ$ $0^\circ \leq \phi \leq 90^\circ$	4	3630	30.25s
Az. angle (fix.) El. angle (var.)	$\theta = 5$ const. vals. $0^\circ \leq \phi \leq 90^\circ$	2	5814	48.45s
El. angle (fix.) Az. angle (var.)	$-40^\circ \leq \theta \leq 90^\circ$ $\phi = 5$ const. vals.	2	6757	56.31s
Random movements	$-40^\circ \leq \theta \leq 90^\circ$ $0^\circ \leq \phi \leq 90^\circ$	N/A	10313	85.94s
Total Frames/Total Time of Mocap Expts.		29551	246.26s	

splines were computed using eq. 3–4. Analysis of this framework using virtual sensing lines was performed in MATLAB. A comparison between real and virtual sensor data is presented in Section IV-B.

The virtual sensor and joint angle data from OpenSim were used to derive the  $\mathbf{q} \mapsto \mathbf{S}$  map and the  $\mathbf{S} \mapsto \mathbf{q}$  map. The  $\mathbf{q} \mapsto \mathbf{S}$  map helps analyse the tendon-routing architecture behaviour (Fig. 4) and is discussed in Section IV-A. This  $\mathbf{q} \mapsto \mathbf{S}$  mapping is also derived using a very shallow ANN network using 1 hidden layer with 8 neurons. The methodology to obtain the  $\mathbf{S} \mapsto \mathbf{q}$  mapping remains the same as was used in [19]. To prepare

the data for neural network-based fitting, the data was scaled globally and shuffled. To train and test the ANN, data from 29,551 frames of MoCap data was used. The ANN was trained on 65% of the data, validated on 15% of the data, and tested on 20% of previously unused data. The results of this mapping is discussed in Section IV-C. The network was developed using the Keras-TensorFlow API in Python 3.5, on an HP Workstation with Intel i7-6700 CPU processor @3.4 GHz with 16 GB RAM.

## IV. RESULTS AND DISCUSSION

### A. Tendon-Routing Architecture Behaviour Analysis

The behaviour of the tendon routing architecture conceptualised in Section II is analysed here. Fig. 4 presents the  $\mathbf{q} \mapsto \mathbf{S}$  mapping of the data from the 4 virtual sensors on moving the shoulder in 2 DoFs. Fig. 4 shows 10% of the sensor values (blue dots) and the ANN-fitted surface. Analysing this mapping is the first step to the actuation framework for the suit. This study is crucial as there are infinite tendon-routing combinations, and even though the sensing tendons can sense during both extending/retracting, actuating tendons can only apply forces when pulling (monotonically decreasing).

We can use the  $\mathbf{q} \mapsto \mathbf{S}$  map (in Fig. 4) to predict if the actuation tendons will displace monotonically and apply the required forces, if the same routing was used for actuation as well. The tendon-routing architecture analysis presented here was further required to isolate the source of the non-monotonic tendon displacement behaviour observed when the same analysis was

performed on the simulation-based study presented in [19]. We hypothesised two potential sources for the non-monotonicity: 1). a sub-optimal tendon-routing architecture, or 2). the limitation in OpenSim which only allowed for markers to be attached to the bones rather than on the skin surface, as would happen in reality. The hypothesis of the tendon-routing architecture being the error source is invalidated in this study.

From Fig. 4, it can be seen that the sensors' behaviour match the behaviour of the equivalent muscles/synergies on which their paths are based. For *e.g.*, it can be seen that during flexion, sensor value  $\text{F}$  monotonically decreases and sensor value  $\text{R}$  monotonically increases, and vice-versa during extension (see cyan and green line in Fig. 4(a)&(d)). This is consistent with the behaviour of the AD, PM, TM and LDo muscles (muscles that influence F/E) on which tendons  $\text{F}$  &  $\text{R}$  have been based. Similarly, during abduction, sensors-SF and SR monotonically decrease (see the magenta line in Fig. 4(b) & (c)). This is consistent with the behaviour of the PD, AD and LD muscles (muscles that influence abduction movements) along which the tendons have been routed. **The increase/decrease in sensor value in Fig. 4 is reflected in the change in colour on the surface plot.** For the HAb/HAd movements as well, the observed sensor data from all 4 sensors conform to the behaviour of the muscles along which they were routed. The results of this movement are shown in the black lines in the 4 subplots of Fig. 4. We can consider these results the validation of our proposed bio-inspired sensing concept. **The red line corresponds to the arm in neutral/rest position and demonstrates Gimbal lock (of this joint angle convention) in DoF-1, as no change in DoF-1 elicits any movement as DoF-2  $\rightarrow 0^\circ$ .**

Some inconsistencies in Fig. 4 are: 1). **The red line in Fig. 4(a) should have been a straight line since it represents the hand in neutral position.** The curve is observed as it is an **extrapolation by the ANN-fitting**. The arm cannot reach  $< 10^\circ$  in that DoF due to the thickness of the suit, and the network makes an estimation in that region. 2) **Some non-monotonicity in the ANN-fitted surface is seen in the top-right corner of Fig. 4(b)&(d).** This is again an extrapolation by the fitting, as that region is out of the arm's workspace (blue dots absent).

### B. Real v/s Virtual Sensing Analysis

To further study our sensing framework, virtual and real sensor values from a movement trial are compared in Fig. 5 & 6. This analysis was done to understand the effects of compliance, friction and other non-linearities encountered by the real tendons **vis-a-vis** the unhindered virtual tendons. This sub-section presents the evolution of:

- 1) real v/s virtual sensors w.r.t time (Fig. 5),
- 2) real v/s virtual sensors w.r.t joint angles (Fig. 6).

The OpenSim graphics in Fig. 5(a) show the movement of the upper-limb in top and front/side view. The trial presented in Fig. 5 is detailed in Table I row 3 where the azimuth angle (DoF-1) is held at different constant values while varying the elevation angle (DoF-2). 5 movements (B-F) are performed in the trial where phase A, B and E represent neutral position, F/E and Ab/Ad respectively.

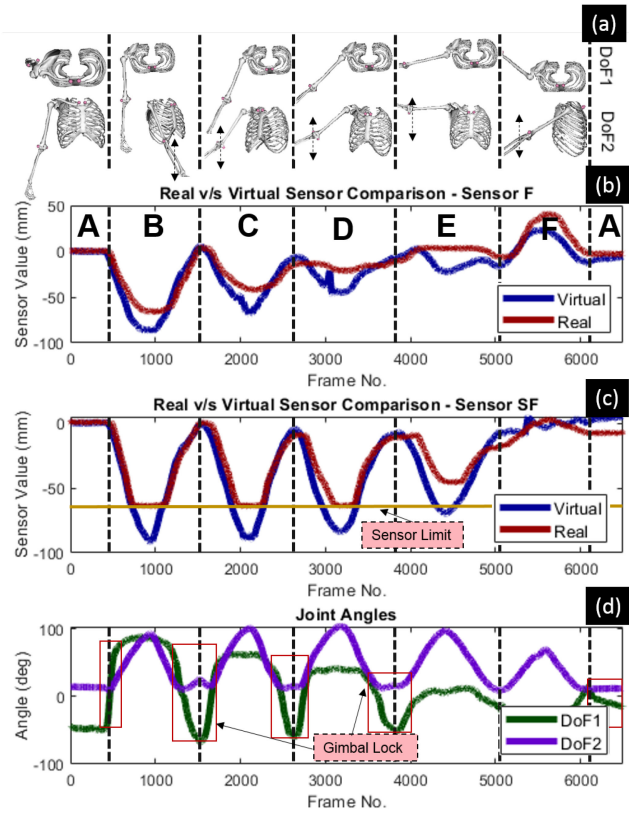


Fig. 5. Comparison of real and virtual sensor performance I: a). Graphics of the top and front view of the pose of the upper-limb during the trial. b)-c). Real and virtual sensor-**F** & **SF** values obtained during the trial. d). DoF-1 & DoF-2 values during the trial. DoF-1 is held constant at a value while DoF-2 is changed from neutral to parallel to ground configuration.

In Fig. 5(b) & (c), we observe that both real and virtual sensors follow the same trend lines for both sensors-**F** & **SF**, and follow the behaviour of their associated muscles/synergies. For **both sensors-**F** & **SF**** (Fig. 5(b) & (c)), we see that the absolute peak value for both real and virtual sensors decrease with decreasing DoF-1 value. For sensor-**F**, the value goes almost to nil during Ab/Ad and changes direction when reverse F/E is performed, while for sensor-**SF**, the value follows the same trend as sensor-**F**, but goes to zero during reverse F/E movement. In sensor-**F**, there is some lag between the virtual and real sensor. This is observed **because the tendon gets pinched near the axillary fossa (armpit)** which increases friction and hinders movement. We intend to correct this in the next iteration by modifying the tendon-routing around the region.

The joint angle representation used for this work is the representation adopted by the MS model [22]. This representation has been used instead of quaternions as it is more intuitive and affords better visualisation of results. The downside of this representation is the **Gimbal lock problem**, and is seen in the sharp change in DoF-1 value as the arm moves to the neutral position (Fig. 5(d)). We intend to use quaternion representation when using this sensing framework for feedback control.

Fig. 6 presents another comparison of the virtual and real sensor values when analysed w.r.t joint angles. Fig. 6 presents the evolution of sensor-**SF** value with changing elevation angle

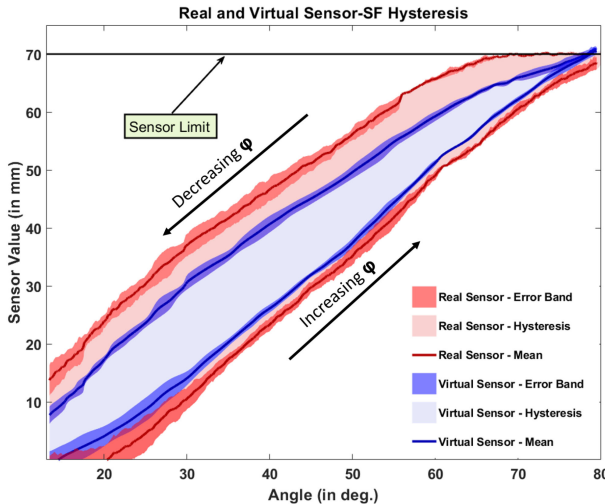


Fig. 6. Comparison of real and virtual sensor performance II: The graph shows the displacement of real (red) and virtual (blue) sensor-SF values against elevation angle during multiple F/E movements. This graph presents the hysteresis and error bands observed in both the real and virtual sensors.

( $\phi$ ) during F/E movements. We can clearly see the existence of hysteresis behaviour in both the real and virtual sensors. In the case of virtual sensors, this behaviour is observed primarily due to the inherent soft nature of the neoprene base suit on which the markers are mounted. In the case of the real sensors, this behaviour is further exacerbated, because of the sensor limit imposed by the termination base (Fig. 6). As previously mentioned, this was done for visual demonstrability of the concept, *i.e.* to visualise tendon displacement as the shoulder moves (see accompanying video). The sensor is not able to recover completely from the imposed sensor limit as we have additional non-linearities introduced by: 1). the friction between tendons and the routing elements, tendon-sheaths, *etc.*, and 2). the local pulling (compliance) exerted by the string-pot and experienced at the termination elements. It is predominantly due to the imposed sensor limit that the tendon experiences a small permanent deformation at the end of sequence of F/E movements. Similar behaviour is observed in other movements as well. The small error band of observed real/virtual sensor values over repeated movements (Fig. 6) demonstrates the repeatability of the framework. We intend to address the friction- and compliance-related shortcomings with adequate design countermeasures in the next version of the suit.

### C. Sensor-to-Joint Space Mapping Performance

This sub-section discusses the performance of the ANN-based  $S \mapsto q$  mapping as presented in Fig. 7. Fig. 7 shows the performance of the  $S \mapsto q$  mapping learned using different networks and varying number of virtual sensors as inputs to the network. The network using all the 4 sensors performed the best followed by comparable performances observed by different combinations of the three sensors. This is followed by the performances of different pairs of sensors. This behaviour is analogous to the behaviour observed in [17] where 4 muscle synergies accounted for more than 90% of the variance in

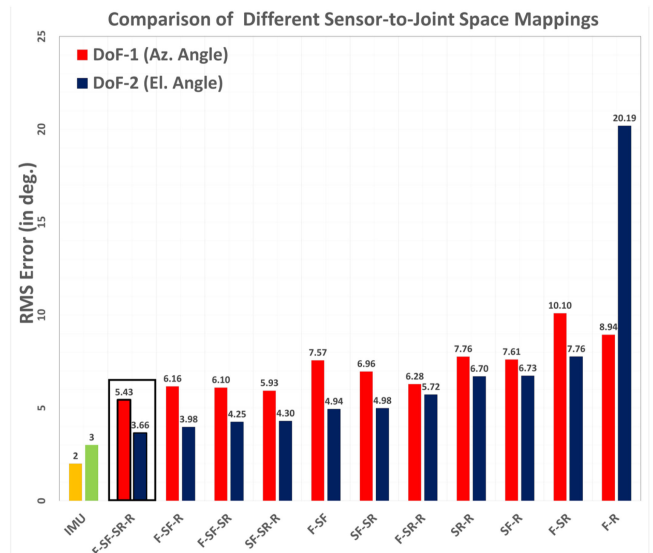


Fig. 7.  $S \mapsto q$  Mapping Performance: RMSE for DoF-1 & DoF-2 for an ANN with 1 hidden layer of 25 neurons. The virtual sensor combination performing the best is encapsulated in the black box. The results for IMU-based solution is shown with orange (DoF-1) and green (DoF-2) bars.

shoulder movements followed by comparable performance by 3 synergies and reduced performance by 2 synergies. In Fig. 7, the **anomaly** is the combination of sensors-F & R, which shows a significantly high RMS error. This is observed because sensors-F & R are almost an **agonist-antagonist** pair, thereby bringing in very similar contributions to the  $S \mapsto q$  map. We can see that a Root Mean Square Error (RMSE) of  $5.43^\circ$  in DoF-1 and  $3.65^\circ$  in DoF-2 was achieved with a network having 25 neurons in the hidden layer and an input from all 4 sensors. These results are promising as we have used a vanilla ANN-based fitting and have achieved RMSE comparable with state-of-the-art IMU-based sensing solutions in DoF-2 [15].

As mentioned earlier, the advantage of our system over state-of-the-art IMU-based solutions is the lack of continuous drift and the ability to use the system in space environments as well, where IMUs could malfunction. From the size perspective, both systems can be very low-profile over the limbs and only require electronics that can be placed inside a backpack. Additionally, another advantage of this framework is the ability to use the sensing tendons as a benchmark for tendons in the actuation system for compensating backlash. Due to the observed hysteresis (Fig. 6), we hypothesise that the results of  $S \mapsto q$  mapping can be further improved with history-based learning and statistical sensor-fusion methods such as Recurrent Neural Networks (RNNs), Long Short-Term Memory (LSTM) networks and Kalman filters.

### V. CONCLUSION

In this work, we present the first step towards a low-profile and wearable multi-DoF shoulder exosuit. Through this work, we attempted to address the challenge of kinematic sensing of a complex joint such as the shoulder where multiple DoFs manifest conjointly. The novel tendon-routing architecture of

our proposed framework takes inspiration from the muscle synergies of the shoulder and proprioception. MoCap experiments were used to validate the performance of our tendon-routing architecture and train an ANN-based mapping from sensor data to joint angles ( $S \mapsto q$ ). The trained ANN with an input from the four sensors achieved a performance with an RMSE of  $5.43^\circ$  and  $3.65^\circ$  in estimating the azimuth and elevation joint angles, respectively.

The prototype presented here proved the feasibility of our proposed bio-inspired tendon-routing architecture. Based on this work, we believe that the tendon-routing architecture can be extended to other multi-DoF joints (such as the hip, wrist and ankle), and also to the actuation framework of the exosuit. The suit was developed and analysed based on the physiology and morphology of one subject, and will be extended to multiple subjects. We intend to investigate methods such as one/few-shot learning and transfer learning to generalise learned mapping from one subject to another and reduce training times. We are also investigating alternative mapping methodologies with non-linearity (friction, hysteresis, creep) estimation solutions such as LSTMs and hysteretic RNNs to improve sensing accuracy. Improved nonlinearity estimation methods would further allow us to replace the current heavier industrial-grade string-pots with lighter nonlinear fabric-, elastomer-, or other soft sensing technologies. The proposed sensing framework (analogous to proprioception) is capable of providing gross motor control and, in the future, will be combined with vision-based sensing modality to facilitate robust fine motor control and teleoperation. In the future, we also intend to extend this concept to sense shoulder internal/external rotation and other multi-DoF joints.

#### ACKNOWLEDGMENT

The authors would like to acknowledge the EPSRC, UK for funding this work. The authors would also like to thank Prof. Etienne Burdet, Shen Treratanakulchai, Dr. Dennis Kundrat, Pierre Berthet-Rayne, Dr. Fani Deligianni, Xu Chen, and Mohamed Abdelaziz for their support with the project, and Dr. Yao Guo, Daniel Freer, Ya-Yen Tsai and Daniel Bautista for their help with MoCap experiments.

#### REFERENCES

- [1] World Health Organization, “Global Health and Aging,” World Health Organization, Tech. Rep., 2011. [Online]. Available: [http://www.who.int/ageing/publications/global\\_health.pdf](http://www.who.int/ageing/publications/global_health.pdf)
- [2] R. J. Varghese, D. Freer, F. Deligianni, J. Liu, and G.-Z. Yang, “Wearable robotics for upper-limb rehabilitation and assistance: A review of the state-of-the-art, challenges and future research,” in *Wearable Technology in Medicine and Health Care*, 1st ed., R. Tong, Ed. Amsterdam, The Netherlands: Elsevier, 2018, ch. 9, p. 340.
- [3] J. C. Perry, J. Rosen, and S. Burns, “Upper-limb powered exoskeleton design,” *IEEE/ASME Trans. Mechatronics*, vol. 12, no. 4, pp. 408–417, Aug. 2007.
- [4] T. Nef, M. Guidali, and R. Riener, “ARMin III - Arm therapy exoskeleton with an ergonomic shoulder actuation,” *Appl. Bionics Biomechanics*, vol. 6, no. 2, pp. 127–142, 2009.
- [5] M. Xiloyannis, L. Cappello, D. B. Khanh, S.-C. Yen, and L. Masia, “Modelling and design of a synergy-based actuator for a tendon-driven soft robotic glove,” in *Proc. 6th IEEE Int. Conf. Biomed. Robot. Biomechatronics*, 2016, pp. 1213–1219.
- [6] P. Polygerinos, Z. Wang, K. C. Galloway, R. J. Wood, and C. J. Walsh, “Soft robotic glove for combined assistance and at-home rehabilitation,” *Robot. Auton. Syst.*, vol. 73, pp. 135–143, Nov. 2015.
- [7] I. Galiana, F. L. Hammond, R. D. Howe, and M. B. Popovic, “Wearable soft robotic device for post-stroke shoulder rehabilitation: Identifying misalignments,” in *Proc. IEEE Int. Conf. Intell. Robots Syst.*, Oct. 2012, pp. 317–322.
- [8] S. Lessard *et al.*, “CRUX: A compliant robotic upper-extremity exosuit for lightweight, portable, multi-joint muscular augmentation,” in *Proc. IEEE Int. Conf. Rehabil. Robot.*, Jul. 2017, pp. 1633–1638.
- [9] K. Xu and D. Qiu, “Experimental design verification of a compliant shoulder exoskeleton,” in *Proc. IEEE Int. Conf. Robot. Autom.*, 2013, pp. 3894–3901.
- [10] N. Li *et al.*, “Bio-inspired upper limb soft exoskeleton to reduce stroke-induced complications,” *Bioinspiration Biomimetics*, vol. 13, no. 6, 2018, Art. no. 066001.
- [11] I. Gaponov, D. Popov, S. J. Lee, and J.-H. Ryu, “Auxilio: A portable cable-driven exosuit for upper extremity assistance,” *Int. J. Control. Autom. Syst.*, vol. 15, no. 1, pp. 73–84, 2017.
- [12] D. Xu, T. A. Gisby, S. Xie, and I. A. Anderson, “Scalable sensing electronics towards a motion capture suit,” *Proc. SPIE*, vol. 8687, Art. no. 86872L, 2013.
- [13] J. B. Chossat, Y. Tao, V. Duchaine, and Y. L. Park, “Wearable soft artificial skin for hand motion detection with embedded microfluidic strain sensing,” in *Proc. IEEE Int. Conf. Robot. Autom.*, 2015, vol. 2015, pp. 2568–2573.
- [14] Y. Mengüç *et al.*, “Wearable soft sensing suit for human gait measurement,” *Int. J. Robot. Res.*, vol. 33, no. 14, pp. 1748–1764, Dec. 2014.
- [15] N. Aslani, S. Noroozi, P. Davenport, R. Hartley, M. Dupac, and P. Sewell, “Development of a 3D workspace shoulder assessment tool incorporating electromyography and an inertial measurement unit preliminary study,” *Med. Biol. Eng. Comput.*, vol. 56, no. 6, pp. 1003–1011, 2018.
- [16] R. H. Fitts, D. R. Riley, and J. J. Widrick, “Functional and structural adaptations of skeletal muscle to microgravity,” *J. Exp. Biol.*, vol. 204, no. 18, pp. 3201–3208, 2001.
- [17] A. Budhota, P. Tommasino, A. Hussain, and D. Campolo, “Identification of shoulder muscle synergies in healthy subjects during an isometric task,” in *Proc. Int. Conf. Rehabil. Robot.*, 2017, pp. 134–139.
- [18] U. Proske and S. C. Gandevia, “The kinaesthetic senses,” *J. Physiol.*, vol. 587, pp. 4139–4146, Sep. 2009.
- [19] R. J. Varghese, X. Guo, D. Freer, J. Liu, and G.-Z. Yang, “A simulation-based feasibility study of a proprioception-inspired sensing framework for a multi-dof shoulder exosuit,” in *Proc. IEEE 16th Int. Conf. Wearable Implantable Body Sensor Netw.*, 2019, pp. 1–4.
- [20] J. A. Winter, T. J. Allen, and U. Proske, “Muscle spindle signals combine with the sense of effort to indicate limb position,” *J. Physiol.*, vol. 568, no. 3, pp. 1035–1046, Nov. 2005.
- [21] G. C. Terry and T. M. Chopp, “Functional anatomy of the shoulder,” *J. Athletic Training*, vol. 35, no. 3, pp. 248–55, Jul. 2000.
- [22] K. R. Saul *et al.*, “Benchmarking of dynamic simulation predictions in two software platforms using an upper limb musculoskeletal model,” *Comput. Methods Biomechanics Biomed. Eng.*, vol. 18, no. 13, pp. 1445–1458, Oct. 2015.
- [23] N. Bernstein, “The co-ordination and regulation of movements: Conclusions towards the study of motor co-ordination,” *Biodynamics Locomotion*, pp. 104–113, 1967.
- [24] A. d’Avella and F. Lacquaniti, “Control of reaching movements by muscle synergy combinations,” *Frontiers Comput. Neurosci.*, vol. 7, p. 42, 2013.
- [25] S. L. Delp *et al.*, “OpenSim: Open-source software to create and analyze dynamic simulations of movement,” *IEEE Trans. Biomed. Eng.*, vol. 54, no. 11, pp. 1940–1950, Nov. 2007.
- [26] X. Xu, J.-H. Lin, and R. W. McGorry, “Coordinate transformation between shoulder kinematic descriptions in the Holzbaur et al model and ISB sequence,” *J. Biomechanics*, vol. 45, no. 15, pp. 2715–2718, 2012.